Vol. 19, No. 2 (2020) 639-652
Revista Mexicana de Ingeniería Química

Rheokinetic and effectiveness during the phenol removal in mescal vinasses with a rotary disks photocatalytic reactor (RDPR)

Reocinética y efectividad durante la remoción de fenol en vinazas de mezcal con un reactor fotocatalítico de discos rotativos (RDPR)

R.S Gines-Palestino[1], E. Oropeza- De la Rosa[1], C. Montalvo- Romero[2], D. Cantú- Lozano[1]*

[1]*Laboratorio de Procesos, División de Estudios de Posgrado e Investigación, Tecnológico Nacional de México-Instituto Tecnológico de Orizaba, Av. Oriente 9 No. 852, Col. Emiliano Zapata, C.P. 94320, Orizaba, Ver., México.*
[2]*Universidad Autónoma del Carmen/Facultad de Química. Ciudad del Carmen, Campeche C.P. 24180, México.*

Received: June 2, 2019; Accepted: September 25, 2019

Abstract

This research shows rheokinetic removal of phenol in mescal distillery residues in a RDPR, using titanium dioxide as semiconductor, with a residence time of 72 h. The highest phenol removal was 82.39% at 55 rpm and 60% (v/v) diluted vinasses; the optimum values were obtained by canonical analysis. Rheological analysis was carried out with a stirrer and Peltier temperature control, and RheoPlus software. Vinasses showed a satisfactory adjustment to Herschel-Bulkley model, rheological index values ($n > 1$) meaning dilatant flow. Temperature dependence models Arrhenius and Poiseuille were carried out. The kinetic analysis was fitted to Langmuir- Hinshelwood. High shear rates at the disks surface and the dilatancy increased vinasses viscosity, promoting the full contact to the semiconductor, increasing the removal efficiency. The effectiveness factor obtained (0.9981) explained that all the reaction is carried out at the catalyst surface. There was rheokinetic correlation found between the initial yield stress and removed concentration.

Keywords: effectiveness, photocatalysis, mescal, rheology, vinasses.

Resumen

Esta investigación muestra la reocinética de la remoción del fenol en vinazas de mezcal con un reactor fotocatalítico de discos rotativos (RDPR), utilizando como semiconductor dióxido de titanio, con un tiempo de residencia de 72 h. La remoción más alta de fenol fue de 82.39% a 55 rpm y 60% (v/v) de vinaza diluida; los valores óptimos se obtuvieron mediante análisis canónico. El análisis reológico se llevó a cabo utilizando la geometría de agitador de paletas rectas, con control de temperatura Peltier y el software RheoPlus. Las vinazas se ajustaron al modelo de Herschel-Bulkley, los valores del índice reológico (n> 1) representan un flujo dilatante. Se llevaron a cabo modelos dependientes de temperatura como Arrhenius y Poiseuille. El análisis cinético se ajustó a Langmuir-Hinshelwood. Las altas tasas de corte en la superficie de los discos y la dilatación aumentaron la viscosidad de la vinaza, promoviendo el contacto total con el semiconductor, aumentando la eficiencia de remoción. El factor de efectividad obtenido (0.9981) muestra que toda la reacción es llevada a cabo en la superficie del catalizador. Se encontró una correlación reocinética entre el esfuerzo de corte inicial y la remoción.

Palabras clave: efectividad, fotocatálisis, mezcal, reología, vinazas.

1 Introduction

1.1 Mescal production in Mexico

Mexico has 76% of the diverse agaves or magueys, and since pre-Hispanic era different species of magueys have been exploited for various uses, one of them being the production of mescal, a distilled alcoholic beverage. In Mexico, mescal production has impacted the daily activities of Mexican communities that over time have given an ecological and economic importance to the mescal production. However, it is also a considerable environmental pollution source due to the organic content in their waste emissions (Martínez, et al., 2019). Mexican distilleries produce nearly 8 million liters of mescal per year. They also make about 90 million liters of mescal vinasses (residues obtained after the fermented sugars by distillation from different agave species).

* *Corresponding author. E-mail*: dencantu@gmail.com
Tel. +52-272-7257056, Fax +52-272-7257056
https://doi.org/10.24275/rmiq/Cat673
issn-e: 2395-8472

This liquid waste of acidic nature is very aggressive toward the environment because of its high volume of toxic and recalcitrant organic matter (Martínez *et al*., 2019). Vinasses contain chemical constituents such as potassium, calcium, magnesium, sulphate, chlorides, lactic acid, glycerol, ethanol, acetic acid and large amounts of phenol, recalcitrant compound considered an undesirable contaminant, because it gives to the unpleasant organoleptic characteristics and it is harmful to human health, among other environmental problems (Croeser *et al*., 2019).

1.2 Advanced oxidation processes

Advanced oxidation processes (AOPs), is an important alternative to remove a wide range of organic compounds, including phenols and dyes (Jaramillo-Páez *et al*., 2018).

The heterogeneous photocatalysis to degrade contaminants is based in using the semiconductor material which absorbs energetic UV-light, for the formation of electrons and holes which are responsible for the formation of active sites on the surface of the semiconductor what promoting the formation of free radicals capable of degrading the contaminants (De Matos Rodrigues *et al*., 2019).

The most used semiconductor is titanium dioxide (TiO_2), which has stood out for its low cost, low toxicity, good mechanical stability and high photocatalytic capacity (Morales-Zarate *et al*., 2018). TiO_2 is sensitive to light that absorbs electromagnetic radiation, mainly in the UV region; It is also an amphoteric oxide, which is very chemically stable. Due to the afore mentioned characteristics, it is the most commonly used photocatalyst to degrade organic molecules during water purification. In order to carry out the support immobilization, TiO_2 synthesis techniques, as that of sol- gel (López-Sánchez, 2010), are used. If there is not proper functioning, the catalyst is poisoned within a few hours. A catalyst can be poisoned by adsorption of impurities in the feed stream, surface fouling and blockage of pores by carbonaceous residues formed as a result of the cracking of some hydrocarbons (Villa-Quezada *et al*., 2018).

Titanium dioxide, being photoactive, allows electron-hole pairs in the conduction band (CB) and positive holes (h+) in the valence band (VB) according to the Eq. (1) (Montalvo-Romero *et al*., 2012).

$$TiO_2 + h\nu \longrightarrow e^-_{CB} + hC^+_{CB} \tag{1}$$

Free radicals ($OH^\bullet$) are formed as shown in Eq. (2) - (3):

$$h^+ + H_2O \longrightarrow OH^\bullet + H^+ \tag{2}$$

$$h^+ + HO^- \longrightarrow OH^\bullet \tag{3}$$

Meanwhile, excess electrons in the conduction band react with molecular oxygen to form superoxide free radicals and hydrogen peroxide, Eq. (4) - (5):

$$O_2 + e^- \longrightarrow {}^\bullet O_2^- \tag{4}$$

$$O_2 + 2H^+ + 2e- \longrightarrow {}^\bullet O_2^- \tag{5}$$

Both superoxide free radical and hydrogen peroxide generate hydroxyl free radical by the Eq. (6) - (9):

$$2\,{}^\bullet O_2^- + 2H_2O \longrightarrow 2HO^\bullet + 2OH + O_2 \tag{6}$$

$$H_2O_2 + O_2^- \longrightarrow OH^- + O_2 + HO^\bullet \tag{7}$$

$$H_2O_2 + e^- \longrightarrow OH^- + HO^\bullet \tag{8}$$

$$H_2O_2 + h\nu \longrightarrow 2HO^\bullet \tag{9}$$

Hydroxyl free radical ($HO^\bullet$) oxidizes and mineralizes completely organic molecules (Moctezuma *et al*., 2016).

1.3 Phenomenology of Rotary Disks Reactor (RDR)

Rotary motions in laminar regime, narrow disposition and high contact surface of the discs promote internal steams, Figure 1 and 2. They reach high velocities of order of Re: 100 which are known as von Kármán streets, (Bird *et al*., 2006) and they promote the total diffusion and fluid impregnation on the semiconductor surface, TiO_2, in both faces of each of six discs. This corresponds to the area per reactor volume, increasing the mass transfer coefficient, and this will influence the efficiency of mass transfer capacity per reactor volume, MEC (Mass transfer Efficiency Capability), according to Eq. (10):

$$MEC = \frac{k_L \cdot a}{P/V}[\equiv] = \frac{h^{-1}}{kW/m^3}[\equiv] = \frac{m^3}{kW \cdot h} \tag{10}$$

where Rotational Disks Reactors-RDR have a MEC = 120, the Continuous Stirred Tank Reactor-CSTR have MEC = 40, (Schürgerl, 1982). This means that the RDR has efficiency 3 times higher than that of CSTR. This is because the fluid is entirely sheared by each revolution of the discs, and the shear rate-rotation speed correlation is $\dot{\gamma}$=N. Cantú-Lozano et al., 2000, reported that Double Screw Helical agitator system present a correlation $\dot{\gamma}$=17.8N. Comparing both correlations, the RDR only needs to accomplish one revolution to cut the fluid and the Double Screw Helical agitator needs 17.8 times to get the fluid cut once; this phenomenology ensures efficient performance of RDR.

According to Fig. 1, the fluid suffers advension due to torsional movements on both faces of the TiO_2 impregnated disk, describing the conical rate profile showed in Fig. 2, which is the way the fluid is contacted; this phenomenon is repeated in each space of the disks.

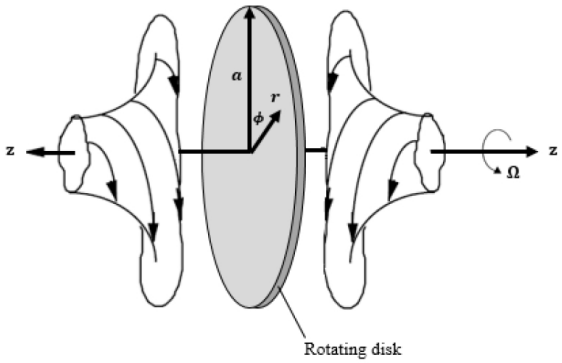

Fig. 1. Von Kármán torsional flows on both sides of an intermediate rotating disc (Adapted from Sohrab, 2005).

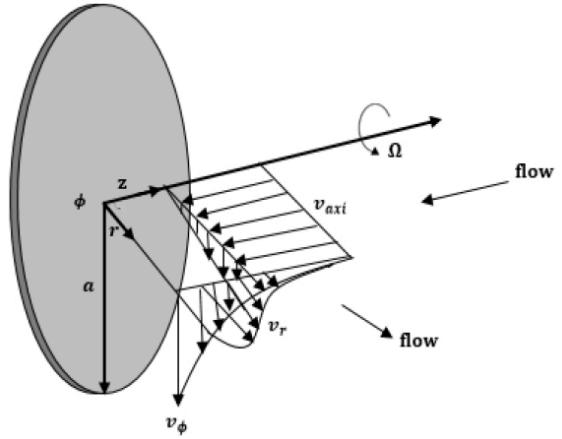

Fig. 2. Rate profile of Von Kármán torsional flows of a rotating disk face (adapted from Shanbghazani *et al.*, 2009).

The phenomenological behavior in the reactor will depend on the vinasses rheological properties. Relevant equations governing the continuity and momentum in RDR, assuming constant thermal physical properties, are Eq. (11) - (18) (Shanbghazani *et al.*, 2009):
Continuity:

$$\frac{\partial v_r}{\partial r} + \frac{v_r}{r} + \frac{\partial v_z}{\partial z} = 0 \tag{11}$$

Momentum:

$$v_r\frac{\partial v_r}{\partial r} + v_z\frac{v_r}{r} - \frac{v_\phi^2}{r} = -\frac{1}{\rho}\frac{\partial p}{\partial r} + \frac{\mu}{\rho}\left(\nabla^2 v_r - \frac{v_r}{r^2}\right) \tag{12}$$

$$v_r\frac{\partial v_\phi}{\partial r} + v_z\frac{\partial v_\phi}{\partial z} - \frac{v_\phi v_r}{r} = \frac{\mu}{\rho}\left(\nabla^2 v_\phi - \frac{v_\phi}{r^2}\right) \tag{13}$$

$$v_r\frac{\partial v_z}{\partial r} + v_z\frac{\partial v_z}{\partial z} = -\frac{1}{\rho}\frac{\partial p}{\partial z} + \frac{\mu}{\rho}\nabla^2 v_\phi \tag{14}$$

where del operator equals: $\nabla^2 = \frac{\partial^2}{\partial r^2} + \frac{1}{r}\frac{\partial}{\partial r} + \frac{\partial^2}{\partial z^2}$
The boundary conditions, figs. 1 - 2, are defined as follows:

- At the disk wall, $z = 0$, $0 \le r \le a : v_r = 0$, $v_\phi\Omega_r$, $v_z = 0$
- At the end of the integration domain, $z = s$, $0 \le r \le a : nu_r = 0$, $v_\phi = 0$, $\partial v_z/\partial r = 0$
- At the disk center, $r = 0$, $0 \le z \le s : v_r = 0$, $v_\phi = 0$, $\partial v_z/\partial r(v_\phi/r) = 0$, $\partial v_z/\partial r = 0$
- At the disk circumference, $r = a$, $0 \le z \le s :$ $\partial/\partial r(v_r/r) = 0$, $\partial/\partial r(v_\phi/r) = 0$, $\partial v_z/\partial r = 0$

Also, the momentum coefficient is defined by Eq. (15):

$$C_m = \frac{M}{0.5\rho\Omega^2 a^5} \tag{15}$$

here, M denotes the frictional moment and it can be expressed as:

$$M = -2\pi\int_a^b r^2\sigma_{\phi,0}dr \tag{16}$$

where: $\sigma_{\phi,0}$ is the shear stress, which for a Newtonian fluid can be calculated from Eq. (17):

$$\sigma_{\phi,0} = \mu\left(\frac{\partial v_\phi}{\partial z}\right)_{z=0} \tag{17}$$

where: μ, is the Newton dynamic viscosity and is defined by Eq. (18):

$$\mu = \frac{\sigma}{\dot{\gamma}} = \frac{\sigma_{\phi,0}}{(\partial v_\phi / \partial z)} \tag{18}$$

where: $\dot{\gamma} = \partial v_\phi / \partial z$, is shear rate or fluid deformation by the disks. Shear stress value, $\sigma_{\phi,0}$, of Eq. (17) will depend on the behavior obtained from the constitutive equation of rheological characterization of vinasses.

From previous studies (Oropeza-De la Rosa, 2013), it has been found that vinasses behavior deviates from Newton's law, Eq. (17), because the dynamic viscosity is not constant. This deviation depends of bioethanol production process. A comparative study of rheological behavior of Mexican and Brazilian sugarcane vinasses, (Cantú-Lozano *et al*., 2010) found that Mexican vinasses, at low shear rates (0-400 s^{-1}) presented pseudoplastic behavior and, in a greater cutting rate range (400-1000 s^{-1}), a turning point with obvious material restructuring manifesting dilatant behavior ($n > 1$) was observed. This behavior was not presented by Brazilian vinasses. Authors attributed the phenomenological behavior difference to the raw material used in each process; in the Mexican process molasses was used as a source of glucose, and in the Brazilian process sugarcane juice was used as a source of glucose.

For these cases Eq. (17) takes the constitutive equation form of Herschel-Bulkley, Eq. (19):

$$\sigma_{HB} = \sigma_{0HB} + K_{HB}(\dot{\gamma})^{n_{HB}} \tag{19}$$

where: σ_{0HB}, is the initial shear stress or yield point. This model and all models that contain this rheological property represent two states of matter: solid and liquid; and initial shear stress or yield point is the border between solid and liquid behavior. From that value vinasses begin to flow. K_{HB}, is the consistency index or non-Newtonian viscosity, and n is the rheological behavior index which indicates how fluid flows. For each point of shear rate it is presented a coefficient denominated apparent viscosity, which is measured by an average value of measurement shear interval, thus combining the Eq. (18) and (19) yields the Eq. (20):

$$\eta_{ap,\dot{\gamma}avg} = \frac{\sigma_{HB}}{\dot{\gamma}} = \frac{\sigma_{0HB}}{\dot{\gamma}} + K_{HB}(\dot{\gamma})^{n_{HB}-1}, \ni n_{HB} > 1 \tag{20}$$

The greater the threshold of rheological behavior index values, n, the greater the distribution of Eq. (20), that is why an average value of $n(\bar{n})$ and shear rate is always chosen, according to Eq. (21).

$$\eta_{ap,\dot{\gamma}avg} = \frac{\sigma_{HB}}{\dot{\gamma}} = \frac{\sigma_{0HB}}{\dot{\gamma}} + K_{HB}(\dot{\gamma})^{\bar{n}_{HB}-1}, \ni \bar{n}_{HB} > 1 \tag{21}$$

1.4 Temperature effect

The consistency index and the apparent viscosity will depend on the temperature in an Arrhenius type exponential form according to Eq. (22):

$$\eta_{ap} = \eta_0 \cdot e^{\frac{E_a}{RT}} \tag{22}$$

where: η_0 is the viscosity at absolute temperature of zero and E_a is the energy required to align the particles and from that point the fluid flows, sometimes called flow activation energy (André *et al*., 2019). Another model used to measure the quadratic dependence of the apparent viscosity with temperature is the Poiseuille model, shown in Eqn. (23) (Michel *et al*., 2018):

$$\eta_{ap} = A + B\left(\frac{1}{T}\right) + C\left(\frac{1}{T}\right)^2 \tag{23}$$

2 Materials and methods

2.1 Chemicals products and reagents

Mescal vinasses from Agaves Mexicanos S.A. de C.V industry, in Matatlán Oaxaca, were used as raw material; this industry belongs to Alimentos TENERIFE S.A. de C.V. For phenol quantification it was used UV-visible spectrophotometry by Folin-Ciocalteu- standard method, using Folin Ciocalteu reagent, phenol, sodium carbonate solutions and sodium tartrate. The reagents used for the solutions were reagent grade.

2.2 Chemical characterization of mescal vinasses

Currently, there is much information regarding sugar, tequila or wine origin vinasses, but very little information about mescal stillage characteristics. It is important to note that the composition of wastewater varies with respect to the raw material used; for such reason it was carried out a chemical characterization of mescal distillery residues in order to obtain relevant information on this type of wastewater.

2.3 Rheological characterization of mescal vinasses

Rheological characterization was performed on an Anton Paar rotational rheometer model MCR301 with a 2.2 cm of diameter stirrer geometry. This was carried out at 4 different temperatures: 20, 40, 60 and 80 °C, controlled with Peltier plate, in order to emulate the temperature at which vinasses are discharged. Data were fitted to the Herschel-Bulkley model Eq. (19) and rheological models depending on temperature: Arrhenius Eq. (22) and Poiseuille Eq. (23). These models described the fluid behavior and data were fitted by RheoPlus software (Oropeza-De la Rosa *et al*., 2019).

2.4 Experimental methods and analysis

In this research, the photocatalytic and rheological conditions necessary for the phenol removal from mescal vinasses with Rotating Disks Photocatalytic Reactor (RDPR) were studied. Fig. 3 shows the corresponding diagram.

Rotating Disks Photocatalytic Reactor -RDPR consists of 4 main components:

- 1 semi cylindrical stainless-steel cover, that holds two ultraviolet lamps with wavelength (λ) of 365 nm and 15 Watts of power. Its dimensions are 41.3 cm long and 17.5 cm.
- 6 Pyrex glass of 24 cm in diameter and 6 mm thick disks, mounted on a stainless-steel shaft of 190.5 mm (3/4 inch) in diameter and 70 cm of longitude. There are two disks placed in each of the reactor´s three used stages with a total operation volume of 6.74 L.
- 1 Cole-Palmer peristaltic pump that maintains a continuous flow from one stage to another of the reaction mixture.
- 1 Elite air supply pump, that provides oxygen within the sample with a flow of 1.0 L O_2 / min.

The titanium dioxide used for this research as a catalyst is commercial, manufactured by Degussa and called P25.

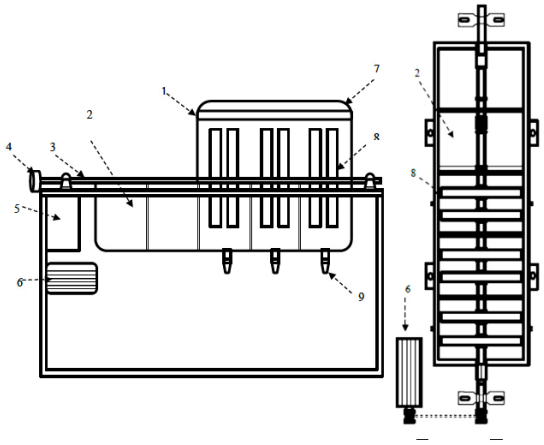

Fig. 3. Rotating Disks Photocatalytic Reactor general diagram. 1. UV lamps; 2. Reactor's body; 3. Axe; 4. Pulley; 5. Electric charge center; 6. Motor; 7. Reactor cover; 8. Rotary disks; 9. Discharge tubes of each stage.

It is used in wastewater treatment where large quantities of photocatalyst are applied at pilot or pre-industrial plant scale. The sol- gel technique was applied for the impregnation of the disks (López-Sánchez, 2010), 10 g of the semiconductor was dispersed in 20 mL of distilled water as a colloidal suspension, this relation was used for the impregnation of a disc. This photocatalyst was already tested in other investigations, using the same photoreactor but with a different sample obtaining phenol removal percentages of 94.4% with synthetic medium (López-Sánchez, 2010) and 87.4% with bioethanol process residue (Oropeza -De la Rosa, 2013). Then a kinetic mathematical model which allowed to determine the course of the reaction was applied; this model accounts for the Langmuir-Hinshelwood isotherm Eq. (24), which was used to determine the value of the reaction constants, k_1, as well as the phenol adsorption equilibrium constant, k_2, over the photo catalyst.

$$-\frac{dC_0}{dt} = -r_0 = \frac{k_1 C_0}{1 + k_2 C_0} \tag{24}$$

where: r_0 is initial reaction speed, C_0 is initial concentration and k_1, k_2 are reaction constant and adsorption constant respectively.

Linearized as Lineweaver-Burk type we have Eq. (25):

$$\frac{1}{-r_0} = \frac{k_2}{k_1} + \frac{1}{k_1 C_0} \tag{25}$$

where: r_0 is initial reaction speed, C_0 is initial

concentration and k_1, k_2 are reaction constant and adsorption constant respectively.

2.5 *Phenol degradation runs in Mescal vinasses*

Phenol degradation was carried out during 72 continuous hours, samples were taken at 0, 1, 2, 3, 5, 9, 17, 25, 33, 41, 49, 57, 65 and 72 reaction hours to monitoring the following parameters: Phenol concentration (APHA, 2005), dissolved oxygen within the reaction, temperature and, concomitantly, the rheological measurements were made. These measurements were done in order to follow the phenomenological behavior of mescal vinasses during phenol removal.

A 22 experimental design with five central points, where phenol removal percentage was the response variable, was performed. The experimental design is shown in Table 1.

The efficiency of phenol photocatalytic degradation in vinasses within the mescal production process was calculated through reported curves, based on the dimensionless number Damköhler Eq. (26), that describes the reactant´s resistance magnitude to diffusion in the catalyst pores, because the pore is small and winding or nearly linear as reported in previous work (Lopez- Sanchez, 2010). The external or surface resistors dominate the system. Note that no matter what the intrinsic surface reaction order may be, in mass-transport-control limit (Da large), the global rate becomes first order i.e. $n = 1$ (Carberry, 1976).

Table 1. Experimental design used for degradation runs.

Factors		***Encoded variables***	
Concentration (% v/v)	*N (Rpm)*	*Dilution (%, v/v)*	*N (Rpm)*
100	80	1	1
100	40	1	-1
10	80	-1	1
10	40	-1	-1
55	60	0	0
55	60	0	0
55	60	0	0
55	60	0	0
55	60	0	0

$$Da = \frac{kC_0^{n-1}}{k_L \cdot a} = Damkhler\ number = \frac{k}{k_L \cdot a} = \frac{chemical - reactionvelocity}{mass - transportvelocity},\ where\ n = 1 \tag{26}$$

where: Da is Damköhler number, k is first order reaction coefficient, $k_L \cdot a$ is Mass transfer coefficient in the liquid phase.

Alternatively, since in general we can express in terms of time: $k = 1/\tau_R$ and $k_L a = 1/\tau_D$ where: τ_R and τ_D are time constants for chemical and diffusive events respectively, so $Da = \tau_D/\tau_R$. Thus, the effectiveness factor ($\bar{\eta}$) for first order surface reaction, considering film as a flat plate L, was calculated with Eq. (27) (Carberry, 1976; Levenspiel, 1989).

$$\bar{\eta} = \frac{global\ rate}{purechemical - reactioncontrol} = \frac{r}{r_0} = \frac{kC_0}{1 + Da}\frac{1}{kC_0} = \frac{1}{1 + Da} \tag{27}$$

where: $\bar{\eta}$ is the effectiveness factor, r_0 is initial reaction speed, C_0 is initial concentration and k is first order reaction coefficient.

2.6 *Rheokinetic correlation*

Previously, it had been found that the variation in the rheological properties and the concentration might correlate with a reliable fit (Cantú-Lozano, 1995). The author found correlations between the relative viscosity and the consistency index with applesauce pulp concentration, Eq. (28) and Eq. (29), at an average shear rate of 100 s^{-1}.

$$\eta_{r,100}^{0.5} = A - \frac{B}{P} \tag{28}$$

$$K^{0.5} = A - \frac{B}{P} \tag{29}$$

where: A and B, are constants, and P is pulp concentration (w/w).

A quadratic equation was applied to correlate vinasses shear stress values during phenol degradation, this type of rheological behavior correlations with chemical kinetics is known as *Rheokinetic* (Cantú-Lozano, 1995).

Table 2. Chemical characterization results of mescal vinasses.

Determination	***Results***
pH[-]	4.07
ρ[g/mL]	1.02143
μ[Pa s]	0.0874
ºBrix	5.91
Color	
L	0.91
A	-0.24
B	-1.04
COD_T	103.17
Phenol	1573.076
X_{TSS}	29.155
X_{VSS}	27.3980

3 Results and discussion

3.1 Chemical characterization of mescal vinasses

Results of chemical parameter determinations are listed in Table 2. Values obtained show that vinasses have an acidic pH, favoring phenolic compounds degradation (López, 2010). The density and viscosity vary depending on the number of suspended solids present in the sample. The analyzed vinasses presented a high content of suspended solids that, according to the regulations, exceed the maximum permissible limits, which are 0.125 g/L (NOM-001-SEMARNAT-1996). Vinasses were not filtered before photocatalytic experiments because it was necessary to know their phenomenological behavior during photocatalytic removal, as they were obtained from the industry. The maximum permissible limit of COD_L T is 0.32 g/L while mescal vinasses presented a value of 103.17 g/L, which has been considered as one of the wastes with a high potential pollution.

Regarding phenol characterization it was found that vinasses contain 1573.076 mg/L when the maximum phenol limit in wastewater discharge is 0.75 mg/L (NOM-CCA-013-ECOL/1993). For this reason, the need to give a treatment to the mescal vinasses is necessary.

The color results of mescal vinasses expressed low brightness value of L = 0.91, due to the dark color of the sample; the a = -0.24 value shows a clear trend to green ("a" negative values indicate green while positive values indicate red); and finally the parameter b = -1.04 shows a blue trend ("b" negative values indicate blue and positive values indicate yellow).

3.1.1 Rheological characterization of mescal vinasses

The results of the rheological characterization showed a non-Newtonian behavior of mescal vinasses with dilatant characteristics ($n > 1$), the flow curves changed noticeably with the shear rate, this occurs especially in concentrated dispersed systems, this behavior is called "structural viscosity"; the fluid rheo-fluidizing at intermediate shear rates, and Newtonian at low shear rates.

In Table 3, it is presented the rheological modeling parameters performed to samples of mescal vinasses fitting to Herschel Buckley constitutive equation with $0.99823 \leq R^2 \leq 0.99936$. According to the Fisher and Yates significance levels (1963), reliability is > 99.9% with an error < 0.1%. It can be seen that the initial shear stress and consistency index decrease with increasing temperature and the rheological behavior index

3.1.2 Arrhenius model

Table 4 shows the decrease in apparent viscosity with respect to temperature at shear rate 500 s^{-1}. In order to obtain the constants values of Arrhenius equation a logarithmic regression was carried out, which is expressed by Eq. (30).

Table 3. Effect of temperature on rheological parameters of Herschel-Bulkley model.

T (°C)	τ_0	**K**	**n**	**Herschel-Bulkley experimental model**	**R^2**
20	13.167	0.0028635	1.4922	$\sigma = 13.167 + 2.8635 \times 10^{-3}\dot{\gamma}^{1.4922}$	0.99936
40	7.8878	0.0012544	1.5891	$\sigma = 7.8878 + 1.2544 \times 10^{-3}\dot{\gamma}^{1.5891}$	0.99875
60	7.4681	0.0015905	1.5434	$\sigma = 7.4681 + 1.5905 \times 10^{-3}\dot{\gamma}^{1.5434}$	0.9988
80	7.1735	0.0007489	1.6372	$\sigma = 7.1735 + 0.7489 \times 10^{-3}\dot{\gamma}^{1.6372}$	0.99823

Table 4. Effect of temperature on apparent viscosity, η_{ap}.

η_{ap} (Pa s) Apparent viscosity	T (K) Temperature
0.0875	293.15
0.065	313.15
0.0619	333.15
0.0544	353.15

$$\ln \eta_{ap} = \ln \eta_0 + \frac{E_a}{R} \cdot \frac{1}{T} \tag{30}$$

The parameters obtained from Arrhenius model are presented in Table 5, which shows the fitting to the model with $R^2 = 0.96064$. According to the Fisher and Yates significance levels (1963) the reliability is > 96% with an error < 0.1%. High activation energy is shown, meaning a greater energy requiring so that vinasses can flow.

3.1.3 *Poiseuille model*

Subsequently another parameter setting via Poiseuille model was conducted, the results are seen in Table 6, where the Poiseuille model presented a higher fitting than Arrhenius model adjustment with $R^2 = 0.982921$. According to Fisher and Yates significance levels (1963) reliability is > 98.2% with an error < 0.1%, this due to the complexity of Poiseuille with a larger number of parameters.

Comparing the Arrhenius and Poiseuille model shown in Table 7, it becomes clear that the setting is higher in this Poiseuille model due to the complexity of the model equation.

3.2 *Phenol degradation*

Obtained removal results were analyzed using statistical software NCSS 2004 in order to obtain the equation that reproduces the phenol removal experimental data, later a canonical analysis was used to determine the optimal conditions for phenol removal (Table 8).

Table 9 shows the experimental design results raised in order to evaluate the interactions. In Figure 4 it is observed that vinasses at 10% under 40 rpm took a slight increase in phenol concentration within the first 30 hours of operation, this due to the intermediate compounds formed like nitro phenols and hydroxyphenols as hydroquinone and resorcinol. During subsequent hours a phenol removal of 42.36% was reached.

Table 5. Arrhenius model parameters.

$\eta_0 \times 10^3$ (Pa s)	E_a (cal/g·mol)	Arrhenius experimental model	R^2
5.98	1.5373	$\eta_{ap} = 5.98 \times 10^{-3} \cdot e^{\frac{1.5373}{RT}}$	0.96064

Table 6. Poiseuille model parameters.

A (Pas)	B (Pas · K)	C (Pas · K^2)	Poiseuille experimental model	R^2
0.04599	0.78448	0.87504	$\eta_{ap} = 0.04599 + (0.78448)\left(\frac{1}{T}\right) + (0.87504)\left(\frac{1}{T}\right)^2$	0.98292

Table 7. Comparison of η_0 with Arrhenius and Poiseuille models.

Parameters	Arrhenius	Poiseuille
$\eta_0 \times 10^3$	5.98	45.99204
R^2	0.92389	0.982921

Table 8. Optimum values of removed phenol obtained through canonical analysis.

N (rpm)	*Dilution (% v/v)*	*Phenol Removed (%)*
80	52	92

Table 9. Results of experimental design.

Factors		***Encoded variables***		***Answer variable***
Dilution (%, v/v)	*N*	*Dilution (%, v/v)*	*N*	*Phenol removed (%)*
100	80	1	1	76.69
100	40	1	-1	26.04
10	80	-1	-1	81.26
10	40	-1	0	42.36
55	60	0	0	80.73
55	60	0	0	78.52
55	60	0	0	80.67
55	60	0	0	81.37
55	60	0	0	82.39

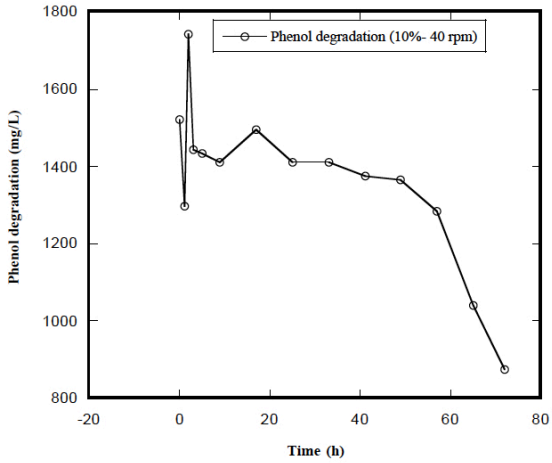

Fig. 4. Phenol degradation at 10% and 40 rpm.

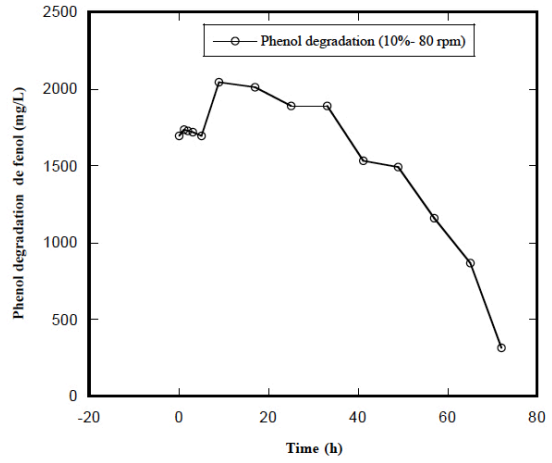

Fig. 5. Phenol degradation at 10% and 80 rpm.

Vinasses at 10% under 80 rpm showed a similar behaviour, figure 5 shows that during the first 30 hours of operation the phenol concentration increased, this due to the presence of intermediate compounds following the same removal behaviour reported in other research with similar operating conditions (López-Sánchez, 2010; Ramirez, 2013; Oropeza-De la Rosa, 2013). During the following hours of degradation, a quick decrease in the phenol concentration was observed. The removal percentage obtained was 81.26%, surpassing the removal percentage obtained under operating conditions 10% and 40 rpm.

The phenol degradation data versus time were successfully fitted to a first order kinetic equation, as it has been reported in the literature (Nikolopoulos *et al*., 2006). The linearized form of the Langmuir-Hinshelwood, Eq. 25, kinetics was used for determining the reaction constant (k_1) and adsorption constant (k_2) trough equation (25), see table 10, which suggests that it is imperative adsorption-desorption equilibrium between the semiconductor surface and the fluid phase so that degradation of any substrate starts. Once the equilibrium is established, the molecule degradation begins by a mechanism involving radicals.

Substituting the Langmuir-Hinshelwood model Eq. (24) with the resulting parameters we obtain the following model, Eq. (31):

$$-r_0 = \frac{9.89\times10^{-3}C_0}{1+1.781\times10^{-5}C_0} \tag{31}$$

With the integration of equation (24) for a first-order kinetics the values of the apparent constant k_{ap} [h^{-1}]were obtained, and multiplying them by the initial concentration of phenol, [mg·L^{-1}]the values of the initial reaction rates r_0[mg·$L^{-1}h^{-1}$] were obtained, see table 11.

Table 10. Values of kinetics parameters of Langmuir-Hinshelwood model.

$\mathbf{k_1 \times 10^3}$	$\mathbf{k_2 \times 10^5}$	R^2
9.89	1.7811	0.913

Table 11. Values of reaction initial rate, r_0.

Initial phenol concentration $[\mathbf{mg \cdot L^{-1}}]$	$\mathbf{k_{ap} \times 10^3}$ $[\mathbf{h^{-1}}]$	$\mathbf{r_0}$ $[\mathbf{mg \cdot h^{-1}L^{-1}}]$
925.087	14.384	13.061
912.946	15.938	14.55
892.713	17.96	16.033
933.18	18.53	17.292
915.981	16.547	15.156
152.073	4.729	0.719
170.081	9.827	1.671
980.488	3.636	3.565

3.3 Effectiveness factor

In order to be able to carry out the calculation of the external effectiveness factor, some data from previous work, Montalvo-Romero, (2000), which are directly related to the same reactor, were required, these data correspond to the values of the coefficient of Transfer of oxygen, $k_L \cdot a[\mathrm{h}^{-1}]$, which at 80 rpm gives a value of 5.28 h^{-1}. Once the oxygen transfer coefficient data was taken, the Damköhler number was calculated by substituting Eq. (26), obtain the following Eq. (32):

$$Da = \frac{9.89 \times 10^{-3} h^{-1}}{5.28 h^{-1}} = 1.873 \times 10^{-3} \qquad (32)$$

The value lower than the unit for the Damköhler number indicates that the resistance to mass transfer is less than the reaction rate. With the Damköhler number the external effectiveness factor was calculated according to Eq. (27), obtain the following result Eq. (33):

$$\bar{\eta} = \frac{1}{1 + 1.873 \times 10^{-3}} = 0.9981 \qquad (33)$$

The effectiveness factor obtained 0.9981 (99.81%), meaning that all the reaction was carried out on the catalyst surface.

Finally, rheokinetic correlation between the yield stress and removed phenol concentration, Eq. (34), with R^2 = 0.98457 for vinasses 100% and 40 rpm is showed in Figure 6. The high shear rates at the disks surface, increased vinasses viscosity, promoting their full contact to the semiconductor and by these means, increasing the removal efficiency.

$$\begin{aligned} &F[mg/L] = -16416 + 2529.6\tau_0 - 89.947\tau_0^2, \\ &R^2 = 0.98457,\ P < 0.05 \end{aligned} \qquad (34)$$

Eq. (34) offers the alternative of knowing the phenol degradation through rheological data, in this case the yield stress. Table 12 shows a comparison of data obtained through Eqn. (34) with a significance level of p < 0.05 and confidence level of > 99.9% (Fisher & Yates, 1963).

$$\begin{aligned} &t = 10.699, t_p = 0.001745, F = 4.344e+04, \\ &F_P < 0.0001,\ \%Average\ Deviation:\ 1.5825 \end{aligned} \qquad (35)$$

Table 12. Comparison of phenol removed experimental values with rheokinetic correlation obtained values.

Reaction time [h]	**Yield stress** σ_0**[Pa]**	**Experimental Values Phenol [mg/L]**	**Obtained values Phenol [mg/L]**	**% Deviation**
1	15.014	1760.2	1738.38	1.2
10	14.359	1723.4	1773.54	-2.9
42	13.563	1747	1714.68	1.85
72	11.734	1152.8	1157.19	-0.38

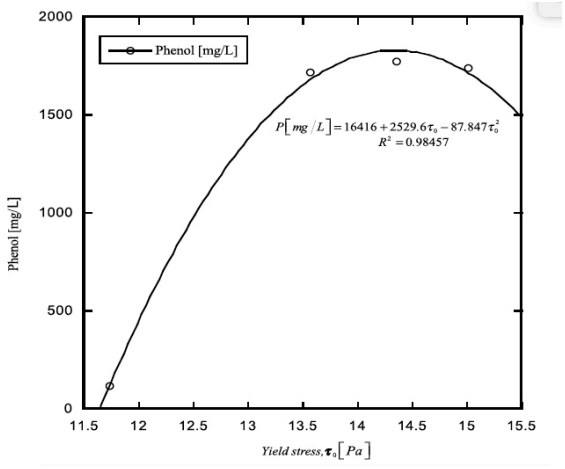

Fig. 6. Rheokinetic correlation between yield stress and phenol concentration to 100% mescal vinasses and 40 rpm of rotational speed, according to Eq. (31).

Conclusions

Photocatalytic degradation runs in the disks rotating reactor showed significant percentages of phenol removal. The vinasses treatment by heterogeneous photocatalysis resulted in a maximum removal rate of 82.39% under the operating conditions of 55% dilution of mescal vinasses at a rotational speed of 60 rpm. Photoreactor design and dilatant rheological behavior of vinasses improved the phenomenological performance of the removal system, being mostly pronounced on the rotating disks surfaces. The analysis indicated that the influential parameter in the Photocatalytic treatment is the rotation speed, since it promotes total contact with the semiconductor. Despite the increase in viscosity, the rotation speed managed to maintain a uniform layer of vinasses on the surface of the discs, the monolayer impregnated in the disc is of a minimum thickness (1 mm), thin enough to receive ultraviolet radiation, increasing the surface area in which ultraviolet light strikes. The higher the number of rpm, the higher the removal percentage. The effectiveness factor obtained was 0.99881, meaning that all the reaction was carried out on the catalyst surface and indicates that the reactor is operating under optimal conditions for phenol removal in mescal vinasses.

The determined rheokinetic correlation offers the alternative of knowing the phenol degradation kinetics in advance, through the rheological data, in this case, the initial shear stress with 99.9% of confidence level.

Acknowledgements

Authors R. S. Gines-Palestino and E. Oropeza-De la Rosa appreciate the support of the National Council of Science and Technology (CONACYT) for scholarships granted with a key number 508410 and 383226 respectively. To Alimentos TENERIFE, S.A. de C.V. México, for donating vinasses samples. We also thank Nuria E. Prado Mora, for the construction of Figures 1 and 2.

Nomenclature

a	contact area per unit volume disks, m^2m^{-3}
A	constant of Eq. (19) dimensionless
A	Poiseuille model constant, Pa s, Eq. (24)
B	Poiseuille model constant, Pa s·K, Eq. (24)
B	constant concentration (w/w), Eq. (19)
C	Poiseuille model constant, Pa s·K^2, Eq. (24)
C	dilution rate of vinasses,%
C_m	momentum coefficient, m^2
C_0	initial concentration, mg·L^{-1}
COD_T	total chemical oxygen demand, gL^{-1}
Da	Damköhler number, dimensionless
E_a	flow energy activation, cal/g·mol
K	consistency index, Pa sn
K_{HB}	consistency index of Herschel-Bulkley model, Pa sn
k_{ap}	apparent constant of reaction velocity, h^{-1}
$k_L \cdot a$	mass transfer coefficient on liquid face, h^{-1}
k	reaction constant of first order, h^{-1}
k_1	reaction constant on liquid face, h^{-1}
k_2	adsorption constant, L·mg^{-1}
MEC	mass transfer efficiency capability, m^3·(kW·h)$^{-1}$
N	rotational velocity, rpm
n	rheological behavior or flow index, dimensionless
$\bar{n}$	average rheological behavior or flow behavior index, dimensionless
P	phenol concentration, mg/L
pH	hydrogen potential, dimensionless
P/V	power input per unit volume, kW/m^3

r_0	initial reaction rate, mg·h^{-1}L^{-1}
X_{TSS}	total suspended solids, g L^{-1}
X_{VSS}	volatile suspended solids, g L^{-1}
t	reaction time, h
ν	rotational velocity, Eq. (11), rpm
V	reactor volume, m^3
Greek symbols	
$\dot{\gamma}$	shear rate, s^{-1}
$\dot{\gamma}_{avg}$	average shear rate, s^{-1}
$\bar{\eta}$	effectiveness factor dimensionless
η_{ap}	apparent viscosity, Pa s.
$\eta_{ap,\dot{\gamma}=500s^{-1}}$	apparent viscosity at shear rate of 500 s^{-1}, Pa s
η_0	apparent viscosity at shear rate of 0 s^{-1}, Pa s
λ	wavelength, nm
μ	dynamic viscosity, Pa s
ρ	density, g L^{-1}
σ	shear stress, Pa
σ_{0HB}	yield stress of Herschel-Bulkley model, Pa
$\sigma_{\phi,0}$	shear stress, Pa, Eq. (17)
Ω	angular velocity, rad·s^{-1}

References

André, S., Leguerinel, I., Palop, A., Desriac, N., Planchon, S., & Mafart, P. (2019). Convergence of Bigelow and Arrhenius models over a wide range of heating temperatures. *International Journal Of Food Microbiology 291*, 173-180.

APHA *Standard Methods for the Examination of Water and Wastewater*. (2005) 21th ed. American Public Health Association. Washington.

Bird, R. B., Stewart W. E., Lightfoot E. N. (2006). *Fenómenos de Transporte*. 2a. Edición. Ed. Reverté, México.

Cantú-Lozano, D., (1995) *Desenvolvimento e utilização de um Agitador Helicoidal de Dupla Hélice como Reômetro*. Tese de Doutorado em Engenharía de Alimentos. UNICAMP, Campinas, Brasil. Pp. 1,

Cantú-Lozano, D., Rao, M.A., Gasparetto, C.A. (2000) Rheological properties of noncohesive apple dispersion with helical and vane impellers: Effect of concentration and particle size. *Journal of Food Process Engineering 23*, 373-385.

Cantú-Lozano, D., Velázquez-Macario, M.V., Vallejo-Cantú, N.A., Mauro, M.A., Del Bianchi, V.L., Telis-Romero, J. (2010) Rheological behaviour of vinasse from a Mexican bioethanol factory. *Proceedings of XXVIIth International Society Sugar Cane Technologists-ISSCT*, Asociación de Técnicos Azucareros de México-ATAM. D.M Hogart ed. (27) March 7-11, Veracruz, México.

Carberry, J.J. (1976). *Chemical and Catalytic Reaction Engineering. Chemical Engineering Series* McGraw-Hill. Pp. 205-207.

Croeser, N., Babaee, S., Naidoo, P., & Ramjugernath, D. (2019). Investigation into the use of gas hydrate technology for the treatment of vinasse. *Fluid Phase Equilibria 492*, 67-77.

De Matos Rodrigues, M., Rodrigues de Sousa, P., Borges, K., de Melo Coelho, L., de Fátima Gonçalves, R., & Teodoro, M. (2019). Enhanced degradation of the antibiotic sulfamethoxazole by heterogeneous photocatalysis using $Ce_{0.8}Gd_{0.2}O_2$-σ/TiO_2 particles. *Journal of Alloys and Compounds 808*, 151711.

Moctezuma, E. Lopez-Barragan, M.A. Zermeño-Resendiz B.B. (2016). Reaction pathways for the photocatalytic degradation of phenol under different experimental conditions. *Revista Mexicana de Ingeniería Química 15*, 129-137.

Fisher & Yates. (1963). *Statistical Tables for Biological, Agricultural and <medical Research* Oliver & Boyd Ltd., Edinburgh, en T. Yamane, Estadística, Tabla 8 Harper & Row, México.

Jaramillo-Páez, C., Navío, J., Hidalgo, M., Macías, M. (2018). ZnO and Pt-ZnO photocatalysts: Characterization and photocatalytic activity assessing by means of three substrates. *Catalysis Today 313*, 12-19.

Levenspiel, O. (1989) *The Chemical Reactor Omnibook*. OSU Book Stores, Inc. Corvallis, Oregon 97339. Pp. 22.3-22.4.

López-Sánchez, G. (2010). *Degradación de fenol en un Reactor Fotocatalítico de Discos Rotativos*.

Tesis de Maestría en Ciencias en Ingeniería Química, Instituto Tecnológico de Orizaba, México.

Martínez, S., Nuñez-Guerrero, M., Gurrola-Reyes, J., Rutiaga-Quiñones, O., Paredes-Ortíz, A., & Soto, O. (2019). Mescal an alcoholic beverage from *agave* spp. with great commercial potential. *Alcoholic Beverages*, 113-140.

Michel, D. (2018). Test of the formal basis of Arrhenius law with heat capacities. *Physica A: Statistical Mechanics and Its Applications 510*, 188-199.

Montalvo-Romero, C. (2000) *Determinación del coeficiente de transferencia de oxígeno (k_L·a) en un reactor de discos rotativos*. Tesis de Maestría en Ciencias en Ingeniería Química, Instituto tecnológico de Orizaba, México.

Montalvo Romero, C., Aguilar Ucán, C.A., Cerón Bretón, J.G. y Cantú-Lozano, D. (2012). *Fundamentos de la Catálisis Heterogénea: Fotocatálisis En: Tópicos Selectos de Ingeniería Química*, Pp. 75-92, ISBN: 978-607-7826-25-5 Universidad Autónoma del Carmen, Campeche, México.

Morales-Zarate, J. A., Paredes-Carrera S.P., Castro-Sotelo, L.V. (2018). Mixed oxides of Zn/Al, Zn/Al-La and Zn-Mg/Al: Preparation, characterization and photocatalytic activity in diclofenac degradation. *Revista Mexicana de Ingeniería Química 17*, 941-953.

Nikolopoulos, A. N., Igglessi-Markopoulou, O. and Papayannakos, N. (2006). Ultrasound assisted catalytic wet peroxide oxidation of phenol: Kinetics and intraparticle diffusion effects. *Ultrasonics Sonochemistry 13*, 92-97.

Oropeza-De la Rosa, E. (2013) *Cálculo de la eficiencia de remoción fotocatalítica de fenol en residuo del proceso de bioetanol (vinazas)*. Tesis de Maestría en Ciencias en Ingeniería Química, Instituto Tecnológico de Orizaba, México.

Oropeza- De la Rosa, E., López-Ávila, L.G., Luna-Solano, G., Urrea-García, G.R., Cantú-Lozano, D. (2019). Dextran treatment and its rheology at bioethanol production process from molasses. *Revista Mexicana de Ingeniería Química 18*, 543-554.

Ramírez, Y.L. (2013) *Diseño, construcción y puesta en marcha de un reactor tubular fotocatalítico (solar/UV-A) CPC para la degradación de desechos químicos orgánicos procedentes de los laboratorios de la escuela de química*. Tesis de Maestría en Química Industrial. Universidad Tecnológica De Pereira, Brasil.

Schürgerl, K. (1982) New bioreactors for aerobic process, international chemical engineering, Oct. 22(4), 591-610. In: *Biochemical Engineering Fundamentals*. Bailey, J.E. and Ollis, D.F. (1986) McGraw-Hill Co. 626-630.

Shanbghazani, M., Heidarpour, V., Mirzaee, I. (2009) Computer-aided analysis of flow in a rotating single disk world academy of science. *Engineering and Technology 58*, 160-161.

Sohrab, S.H. (2005) A Modified Theory of Laminar Flow Near a Rotating Disk http://www.mech.northwestern.edu/dept/people/faculty/sohrab.html p. 3.

Villa-Quezada, J. I., García, L., López, C.M., Mora-Quezada, S.A., García A. (2018). Evaluation of solid catalysts used in petroleum refinery and its regeneration potential. *Revista Mexicana de Ingeniería Química, 17*, 927-940.